Cardiovascular Diabetology

ORIGINAL INVESTIGATION

Open Access

Liraglutide preserves CD34$^+$ stem cells from dysfunction Induced by high glucose exposure

Annalisa Sforza[1†], Vera Vigorelli[1†], Erica Rurali[1], Gianluca Lorenzo Perrucci[1], Elisa Gambini[1], Martina Arici[2], Alessia Metallo[2], Raffaella Rinaldi[1], Paolo Fiorina[3,4,5], Andrea Barbuti[6], Angela Raucci[7], Elena Sacco[2], Marcella Rocchetti[2], Giulio Pompilio[1,8], Stefano Genovese[9†] and Maria Cristina Vinci[1*†]

Abstract

Background: Glucagon like peptide-1 receptor agonists (GLP-1RAs) have shown to reduce mortality and cardiovascular events in patients with type 2 diabetes mellitus (T2DM). Since the impairment in number and function of vasculotrophic circulating CD34$^+$ hematopoietic stem progenitor cells (HSPCs) in T2D has been reported to increase cardiovascular (CV) risk, we hypothesized that one of the mechanisms whereby GLP-1 RAs exert CV protective effects may be related to the ability to improve CD34$^+$ HSPC function.

Methods: In cord blood (CB)-derived CD34$^+$ HSPC, the expression of GLP-1 receptor (GLP-1R) mRNA, receptor protein and intracellular signaling was evaluated by RT-qPCR and Western Blot respectively. CD34$^+$ HSPCs were exposed to high glucose (HG) condition and GLP-1RA liraglutide (LIRA) was added before as well as after functional impairment. Proliferation, CXCR4/SDF-1α axis activity and intracellular ROS production of CD34$^+$ HSPC were evaluated.

Results: CD34$^+$ HSPCs express GLP-1R at transcriptional and protein level. LIRA treatment prevented and rescued HSPC proliferation, CXCR4/SDF-1α axis activity and metabolic imbalance from HG-induced impairment. LIRA stimulation promoted intracellular cAMP accumulation as well as ERK1/2 and AKT signaling activation. The selective GLP-1R antagonist exendin (9–39) abrogated LIRA-dependent ERK1/2 and AKT phosphorylation along with the related protective effects.

Conclusion: We provided the first evidence that CD34$^+$ HSPC express GLP-1R and that LIRA can favorably impact on cell dysfunction due to HG exposure. These findings open new perspectives on the favorable CV effects of GLP-1 RAs in T2DM patients.

Keywords: GLP-1 receptor agonist, CD34$^+$ hematopoietic stem progenitor cells, Type 2 diabetes mellitus, Cardiovascular disease

Background

Type 2 diabetes mellitus (T2DM) has now attained the status of a global pandemic with over 400 million individuals affected worldwide [1]. Despite glucose lowering therapies, mortality from cardiovascular disease (CVD) remains high and extremely costly for health care systems both in terms of medical expenses and disability-adjusted life years [2]. For these reasons, the development of new

*Correspondence: cristina.vinci@ccfm.it
†Annalisa Sforza and Vera Vigorelli equally contributed as first author
†Stefano Genovese and Maria Cristina Vinci equally contributed as last author
[1] Unit of Vascular Biology and Regenerative Medicine, Centro Cardiologico Monzino IRCCS, Via C. Parea 4, 20138 Milan, Italy
Full list of author information is available at the end of the article

therapeutic strategies able to prevent CVD morbidity and mortality is crucial. Patients with T2DM are characterized by a significant decrease in circulating $CD34^+$ stem/progenitor cells. $CD34^+$ hematopoietic stem/progenitor cells (HSPCs) are known to possess vascular regenerative and proangiogenic capacity [3]. Their functional and numerical depletion is now considered a significant contributor to CV homeostasis impairment in diabetes. To this regard, Fadini et al. demonstrated that $CD34^+$ HSPCs are reduced of about 40% in T2DM [4], and that such impairment contributes to enhanced CV risk [5]. Notably, in patients with T2DM, the reduction of $CD34^+$ HSPCs number and function predicts adverse CV outcomes, defined as major CV events (MACE), and hospitalizations for CV causes [6, 7]. Recent large-scale trials have unequivocally demonstrated the ability of glucagon-like peptide 1 receptor agonists (GLP1-RAs) to reduce the risk of MACE in T2DM patients with established or at high risk of CVD [8–10]. GLP1-RAs are now recommended by guidelines as first-line agent for prevention of CVD in T2DM patients [11, 12]. Such pleiotropic CV benefit appears to be additional to glucose-lowering effects and the mechanisms whereby they exert such striking CV protective effects are still largely unknown. At cellular and molecular level, GLP1-RA effects are mediated by GLP1-R, a Gs coupled receptor family member, which is present in various human tissues [13]. To date, there are no data describing the effects of GLP1-RAs on $CD34^+$ HSPCs of T2DM patients. We hypothesized that at least part of the unknown mechanisms whereby GLP1-RAs exert CV protective effect are mediated by its ability to improve $CD34^+$ HSPC function. Here, by exploiting an in vitro model of diabetes, we show for the first time that $CD34^+$ HSPCs express GLP-1R and that its stimulation by liraglutide (LIRA), a GLP1-RA, prevents and recovers the dysfunction induced by hyperglycemia.

Methods

Experimental design

We recently established a stem cell culture model of diabetes based on the use of cord blood (CB)-derived $CD34^+$ HSPCs [14]. This method already provided a consistent and reproducible recapitulation of the major $CD34^+$ HSPC dysfunction hallmarks in diabetes [14]. To assess the ability of GLP-1 RA to prevent $CD34^+$ HSPC dysfunction induced by glucose overload the cells were expanded in high glucose (HG; 30 mM) conditions along with 50 nM or 100 nM LIRA treatment (Fig. 1A). In a different experimental setting, $CD34^+$ HSPCs were expanded in HG condition and then treated with LIRA only after loss of glucose tolerance (Fig. 1B). Afterwards, we assessed the ability of the drug to recover a compromised phenotype. $CD34^+$ HSPCs cultured in normoglycemic condition (NG; 30 mM mannitol) were used as control. At the end of both experiments, the main dysfunctional hallmarks of the cells, namely proliferation and CXCR4/SDF-1α axis impairment, were evaluated (Fig. 1).

Cell culture

Umbilical cord blood (UCB) was collected from the umbilical cord of full-term normal deliveries in collaboration with Milano Cord Blood Bank (IRCSS Ca' Granda Foundation – Ospedale Maggiore Policlinico). The mononuclear cell fraction was obtained by density gradient centrifugation using Ficoll-Paque (Lymphoprep, Sentinel Diagnostics) and $CD34^+$ HSPCs were immunomagnetically isolated using CD34 Microbead Kit (MiniMACS kit, Miltenyi Biotec). Flow-cytometric analysis allowed to assess the purity of sorted cell population, displaying 90% of $CD34^+$ HSPCs and negligible presence of $CD14^+$ (monocytes) and $CD3^+$ (lymphocytes) cells (Additional file 1: Figure S1). Isolated $CD34^+$ HSPCs were cultured in Stem Span medium (StemCell Technologies) supplemented with 20 ng/mL of interleukin (IL)-6 (PeproTech), 20 ng/mL of IL-3 (PeproTech), 50 ng/mL of fms-like tyrosine kinase 3 (FLT3, PeproTech), and 50 ng/mL of stem cell factor (SCF, PeproTech). Cells were cultured in HG (30 mM of glucose, Sigma-Aldrich) or NG (30 mM of mannitol, Sigma-Aldrich) conditions for up to 20 days and treated or not with increasing concentration of LIRA (50 nM and 100 nM; MedCHemExpress) ± selective GLP-1R antagonist exendin (9-39) (150 nM EXE; MedCHemExpress).

Capan-1 cells (HTB-79™), used as GLP-1R positive control, were purchased from ATCC and grown in RPMI medium supplemented with 20% FBS, as indicated by the supplier.

Isolation of $CD34^+$ HSPCs from patient bone marrow

$CD34^+$ HSPCs were isolated from sternal bone marrow (BM) biopsy of T2DM patients underwent bypass surgery. During surgical procedure, 2 mL of sternal BM blood were withdrawn by biopsy needle (15G × 25/90 mm; MDL) and suspended in saline buffer solution. BM-derived $CD34^+$ HSPCs were isolated as aforementioned and collected for GLP-1R mRNA analysis.

All experiments were carried out upon approval of local ethic committees (CCM 205–RE 3428) and informed written consent was obtained from all patients before BM harvesting.

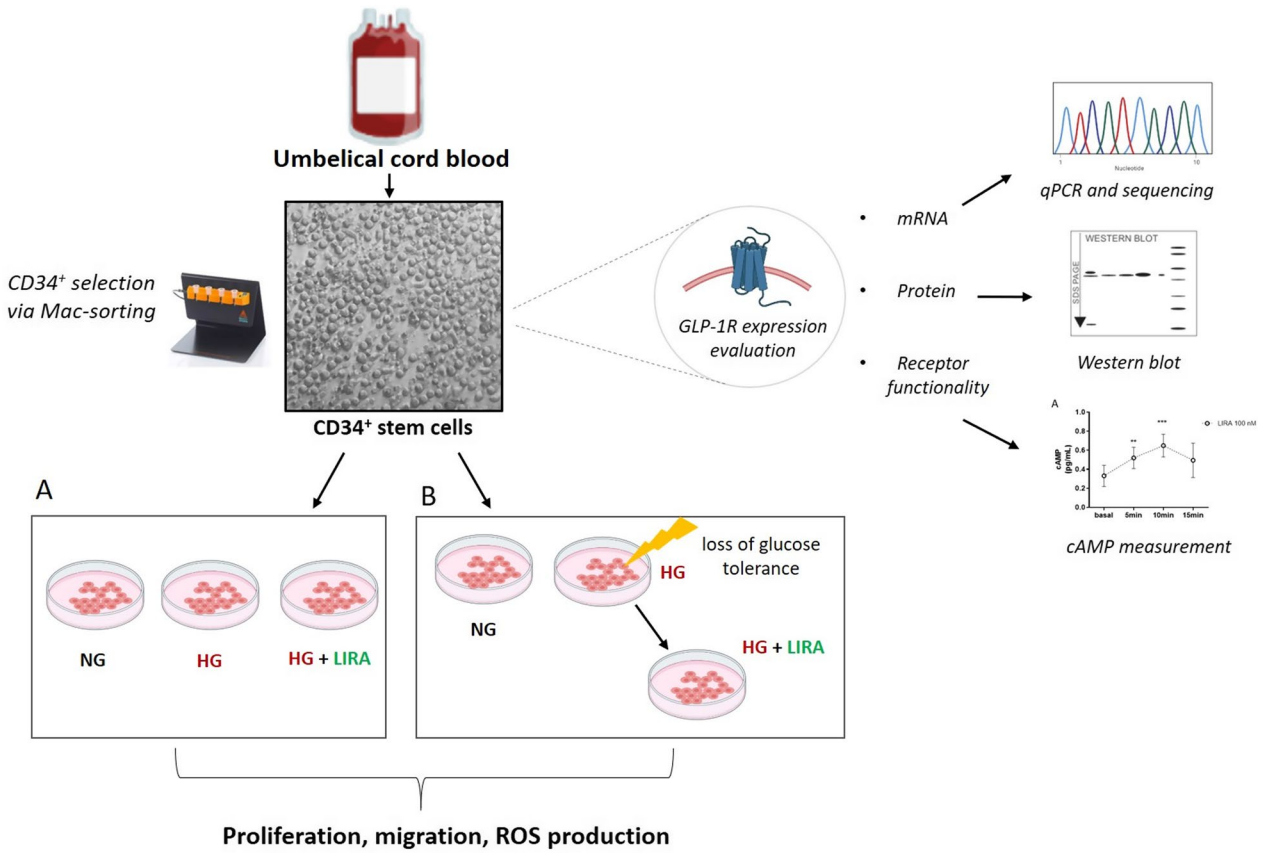

Fig. 1 Schematic representation of the study. CD34$^+$ HSPCs were isolated via Mac-sorting from cord blood and characterized for GLP-1R transcript and protein expression levels, and downstream signaling pathway activation. Then, CD34$^+$ HSPCs were expanded in HG condition with or without LIRA (**A**). In a different experimental setting the cells were treated with LIRA only after the loss of glucose tolerance (**B**). CD34$^+$ HSPCs cultured in NG (30 mM mannitol) condition were used as control (**A**, **B**). Proliferation, migration and oxidative stress were finally assessed at the end of experiments. GLP-1R = glucagone-like peptide 1 receptor; HG = high glucose; LIRA = liraglutide; NG = normal glucose

Cell proliferation assay

CD34$^+$ HSPCs were seeded at an initial density of 2.0×10^5 cells/well and cultured for up to 20 days in NG and HG ± LIRA conditions. Cells were counted on days 5, 10, 15 and 20. Doubling time was calculated with the following formula:

$$\text{Doubling time: } \frac{duration\ x\ \log\ (2)}{\log\ (final\ concentration) - \log\ (initial\ concentration)}$$

Migration assays

Cell migration was determined the use of Boyden modified chamber consisting of transwell culture inserts (5-µm pore membrane; Corning Incorporated, Corning, NY). In brief, 1×10^5 cells were seeded onto the upper chamber and allowed to migrate toward the lower chamber containing, or not, stromal cell-derived factor 1 (SDF-1α 50 ng/mL; PeproTech EC Ltd.). The transwells were incubated at 37 °C, 5% CO_2, for 4 h. Migrated cells in the lower chamber were counted and migration index were calculated with the following formula:

$$\text{Migration index: } \frac{migrated\ cells\ in\ presence\ of\ SDF - 1a}{migrated\ cells\ in\ absence\ of\ SDF - 1a}$$

Cyclic adenosine monophosphate (cAMP) quantification

Intracellular cAMP was quantified by cAMP ELISA kit (Enzo Life Science) according to manufacturer's instructions. Briefly, 5×10^5 CD34$^+$ HSPCs were stimulated with LIRA ± EXE and lysed in 0.1 M HCl and 0,1% Triton X-100. Sample absorbance was spectrophotometrically evaluated at 405 nm by Tecan (Infinite M200 Pro, TECAN).

Intracellular Ca^{2+} handling

The measurement of intracellular Ca^{2+} has been assessed through single cell and population analysis by means of confocal Nikon A1R microscope and FLUOstar Omega (BMG Labtech) multiplate reader respectively. $CD34^+$ HSPCs were starved for 2 h (with IMDM and albumin 0.1%) and incubated with the Ca^{2+-}sensitive dye Fluo-4 AM (ThermoFisher, 2 μM) in Tyrode's solution (containing in mM: 154 NaCl, 4 KCl, 2 CaCl2, 1 MgCl2, 5 HEPES/NaOH, and 5.5 d-glucose, adjusted to pH 7.35) for 1 h.

Confocal single cell analysis was performed by plating $CD34^+$ HSPCs on fibronectin/polylisin D coated glass coverslips; fluorescence (F) images (512*512 pxls) were acquired at × 60 magnification every 5 s in basal condition and following 100 nM LIRA addition at 37 °C and 5% CO2 thanks to Okolab incubator mounted on the microscope stage. Changes in single cell mean F during acquisition time were quantified through NIS-Elements analysis software following F backgroud subtraction. Population analysis was performed by plating cells in 96-well dark plates by means of the multiplate reader equipped with an automatic injection system to inject LIRA (100 nM). F was acquired in each well every 0.74 s for 20 s just prior to compound injection and for 100 s after injection. Mean F prior compound injection was used as reference (F0) for signal normalization (F/F0).

RNA extraction and RT-qPCR

Total RNA from both cord-blood and sternal $CD34^+$ HSPCs was isolated by using the Direct-zol RNA Kit (Zymo Research), following manufacturer's protocol. One μg of total RNA was converted to cDNA with the Superscript III kit (Life Technologies) and used to assess GLP-1R gene expression. qPCR reactions were performed with SYBR Green Supermix 2X (BIO-RAD Laboratories) on CFX96 Real–Time System PCR (BIO-RAD Laboratories). Specific GLP-1R primers (Fw: 5'-GTG TGGCGGCCAATTACTAC-3'; Rv: 5'-CTTGGCAAG TCTGCATTTGA-3') were appositely designed to evaluated mRNA expression by amplifying a region of 347 bp. The qPCR products were loaded on a 1% agarose gel with an appropriate molecular marker (PCR Marker Solution, Sigma-Aldrich). Then, the 347 bp bands were excised and purified with QIAquick Gel extraction kit (Qiagen) for subsequent Sanger sequencing analysis.

Sanger sequencing

The RT-qPCR products, appropriately purified from agarose, were sequenced with the help of an external service (Microsynth Biotech) by Sanger method with the use of GLP-1R Fw primer. Sequencing results were analysed by a Multiple sequence ClustalW alignment (BioEdit software) throughout the comparison of the published GLP-1R cDNA sequence (NCBI Reference sequence: NM_002062.5).

Western blot

$CD34^+$ HSPCs and Capan-1 cells were lysed in lysis buffer (50 mM TRIS-HCl, 150 mM NaCl, 1 mM EDTA, 1% Triton) added with protease inhibitors (1:10, Halt Protease Inhibitor Cocktail, Thermo Scientific). Protein lysate was then quantified by Pierce™ BCA Protein Assay Kit (ThermoFisher Scientific). Fourty μg and 20 μg of protein from $CD34^+$ stem cells and capan-1 cells respectively were resolved on 10% SDS-PAGE in denaturing conditions. Proteins were then transferred onto a polyvinylidene difluoride (PVDF) membrane (Millipore) at 400 mA, 4 °C for 90 min. To prevent aspecific binding, the membrane was blocked with 5% bovin serum albumin (BSA) in PBS + 0, 1% Tween-20 (PBST) for 1 h. The membranes were then incubated with the primary antibodies, appropriately diluted in 3% BSA-PBST, at 4 °C O/N and with the appropriate secondary antibody linked to horseradish peroxidase (HRP) the day after for 1 h. Specific information about antibodies and appropriate dilutions are reported in Table 1. The signal was detected by Enhanced chemiluminescence (ECL) system and quantified by Chemidoc MP Imaging System (BIO-RAD Laboratories). GLP-1R-mediated AKT and ERK1/2 pathway activation was evaluated by treating the cells with 100 nM LIRA ± 1 μM wortmannin (Sigma Aldrich; WT; inhibitor of phosphatidylinositol 3-kinase, PI3K), 100 μM PD 98059 (Sigma Aldrich; PD; a specific inhibitor of mitogen-activated protein kinase kinase 1/2, MEK1/2), or 150 nM EXE (selective GLP-1R antagonist) and with either no additions as control.

Table 1 List of Western blot antibodies

	Code (purchased from)	Source	Dilution
Primary antibody			
GLP-1R (D-6)	Sc-390774 (Santa Cruz Biotecnology)	Mouse	1:200
Phospho-p44/42 MAPK (ERK1/2) (Thr202/Tyr204)	#4370 (Cell signaling)	Rabbit	1:2000
p44/42 MAPK (ERK1/2)	#9102 (Cell signaling)	Rabbit	1:1000
Phospho-AKT (Ser473)	#9271 (Cell signaling)	Rabbit	1:1000
Secondary antibody			
ECL Anti-rabbit IgG	NA9340 (Amersham Biosciences)	donkey	1:10000
ECL Anti-mouse IgG	NA9310 (Amersham Biosciences)	sheep	1:5000

Flow cytometric assays

$CD34^+$ HSPCs were incubated for 30 min with allophycocyanin-conjugated monoclonal antihuman CXCR4 antibody (BD Biosciences) or with CellROX Green Flow Cytometry Assay Kit (Life Technologies) for the detection of CXCR4 and reactive oxygen species (ROS) respectively. The Gallios Flow Cytometer platform (Beckman Coulter Life Sciences) was used to analyze the samples after appropriate physical gating. At least 20^4 events in the indicated gates were acquired.

Immunocytochemistry

$CD34^+$ HSPCs were temporarily adhered to a glass coverslip surface by mixed fibronectin-polylysine D (1:1) coating solution. Immediately after adhesion, cells were incubated with Green CellROX (Life Technologies) for 20 min and then fixed with 2% paraformaldehyde solution. Before mounting, cells were counterstained with Hoechst for the nuclei (1:1000) and Wheat Germ Agglutinin for the cell membrane (WGA) (1:200). The images were acquired by ZEISS Apotome fluorescence microscope at 40X magnification.

Analysis of mitochondrial and glycolytic bioenergetic parameters

Bioenergetic parameters were analyzed by using Seahorse XFe96 Extracellular Flux analyzer (Agilent). Before the analysis, cells were collected and counted: 35×10^3 cells were suspended in 50 µL low buffered DMEM-based XF assay medium (103575-100 Agilent) supplemented with 10 mM glucose, 2 mM glutamine, 1 mM Na-pyruvate, and plated in a fibronectin-polylysine D coated 96-well XF plate (Agilent). The XF plate was centrifuged at 200 g (zero braking) for 1 min and incubated for 20 min at 37 °C in a no-CO_2 incubator. Before testing, 150 µL complete XF assay medium was added to each well and cells were furtherly incubated for 30 min at 37 °C.

Mitochondrial bioenergetic parameters were analyzed according to the Seahorse Mito Stress test kit protocol (Agilent) that include oxygen consumption rate (OCR; pmolO_2/min) measurements under basal condition and after the sequential injection of the ATP synthase inhibitor oligomycin A (1.5 µM), the ETC accelerator ionophore FCCP (carbonilcyanide p-triflouromethoxyphenylhydrazone, 2 µM), and the ETC inhibitors mixture rotenone (0.5 µM) + antimycin A (0.5 µM). The minimal doses of oligomycin A and FCCP causing the maximal response used in the Mito Stress test assay were determined for each experimental group in a preliminary Seahorse assay (Additional file 2: Figure S2).

Glycolytic bioenergetic parameters were analyzed by combining the Seahorse ATP rate and Glyco rate test kit protocols (Agilent) including extracellular acidification rate (ECAR; mpH/min) measurements under basal condition and after the sequential injection of 1.5 µM oligomycin A, 0.5 µM rotenone + 0.5 µM antimycin A mixture, and finally 50 mM 2-Deoxy-D-Glucose (2DG).

Seahorse parameters were normalized to cell number in each well. To this purpose, at the end of the Seahorse analysis, cell nuclei were marked with Hoechst 33342 (1 µg/mL) for about 15 min and acquired with Leica Thunder Imager microscope through a 10x objective. Cell number was quantified through ImageJ software. Samples were analyzed with at least 10 technical replicates from two independent experiments. Bioenergetic parameters were calculated from the Seahorse data using Wave2.6.1 (Agilent) software.

Respiratory parameters were calculated using the following formulas:

Basal Mitochondrial Respiration (Basal MR) = OCR under basal condition (OCR_{basal})–OCR following rotenone/antimycin A injection ($OCR_{rot/ant}$); Maximal MR (Max MR) = OCR following FCCP injection (OCR_{FCCP}) − $OCR_{rot/ant}$; Spare respiratory capacity = Max MR–Basal MR; Coupling efficiency = delta OCR following oligomycin A injection (OCR_{basal}-OCR_{oligo})/OCR_{basal}; Proton Leak = OCR_{oligo}-$OCR_{rot/ant}$.

Glycolytic parameters were calculated using the following formulas:

Proton Efflux rate (PER; pmolesH^+/min) was calculated from Extracellular Acidification Rate (ECAR) applying the Buffer Factor of the XF assay medium; Basal glycolysis = PER under basal condition (PER_{basal})–PER following 2DG injection (PER_{2DG}); Maximal glycolysis = PER following rotenone/antimycin A injection ($PER_{rot/ant}$)–PER_{2DG}.

ATP rate parameters were calculated using the following formulas:

ATP linked respiration (OCR_{ATP}) = OCR_{basal}–OCR_{oligo}; mitoATP production rate = OCR_{ATP} *2 * P/O (P/O = 2.75); mitoOCR = OCR_{basal}–$OCR_{rot/ant}$; mitoPER = mitoOCR * CO_2 Contribution Factor (CCF = 0.61); PER = ECAR * Buffer Factor * VolXF microchamber * Kvol (Kvol = 1.6); glycoATP production rate (glycoPER) = PER–mitoPER.

Statistical analysis

Results are given as mean ± SEM. All experiments were performed at least in triplicate, unless stated otherwise. The data were tested for the normality by using the Shapiro–Wilk normality test. Differences between data were evaluated by 1-way, 2-way repeated-measures ANOVA followed by the post-hoc Newman–Keuls or Tukey's multiple comparison test, as appropriate. A value of $P \leq 0.05$ was considered significant. All statistical analysis

was performed using GraphPad Prism software (GraphPad Software Inc.).

Results

CD34$^+$ HSPCs express GLP-1 receptor

We profiled the expression of GLP-1R in CD34$^+$ HSPCs at both mRNA and protein levels. In order to ensure cDNA amplification of the target mRNA and exclude PCR products from DNA contamination, we designed a couple of primers spanning exon-exon junction (Fig. 2A). Additionally, to confirm the correct amplification of the target template, the amplicon of 347 bp, characterized by a melting temperature of 83 °C, was resolved on 1% agarose gel. The bands were then excised and sequenced. The alignment of sequenced PCR end-point products with reference coding cDNA (NM_002062.5) showed 99% of identity (Fig. 2B, C and D). Additionally, in order to further support our hypothesis, GLP-1R mRNA expression was confirmed in CD34$^+$ HSPCs isolated from sternal BM biopsy of T2DM patients underwent bypass surgery (Additional file 3: Figure S3). Finally, total protein cell lysates obtained from 3 different samples of CD34$^+$ HSPCs were subjected to Western blot analysis. Protein cell lysate of capan-1 cells was used as positive control. As shown in Fig. 1E, GLP-1R antibody detected a unique, distinct protein band of the expected molecular weight (55 kDa) in all samples.

The administration of GLP-1 receptor agonist LIRA stimulates intracellular cAMP production

GLP-1Rs are known to be coupled to activation of Gαs proteins. In pancreatic β cells the receptor agonist engagement results in activation of adenylate cyclase with consequent production of 3',5'-cyclic adenosine monophosphate (cAMP), intracellular Ca^{2+} increase and insulin release [15]. To determine whether CD34$^+$ HSPCs express a functional GLP-1R, we assessed intracellular cAMP production and Ca^{2+} mobilization after LIRA stimulation.

Consistent with activation of Gαs, the treatment of cells with LIRA elicited a significant accumulation of intracellular cAMP over basal level in a time- and dose dependent manner reaching the highest value after 10 min of stimulation at 100 nM (Fig. 3A and B). Notably, the addition of the selective GLP-1R antagonist exendin (9-39) (EXE) prevented intracellular cAMP accumulation at all tested LIRA concentrations, demonstrating a receptor-mediated effect (Fig. 3B). Interestingly, single cell analysis showed occurrence of spontaneous Ca^{2+} transients in CD34$^+$ HSPCs not significantly altered by 100 nM LIRA addition (Additional file 4: Figure S4A). Moreover, cell population analysis showed negligible increase in intracellular Ca^{2+} following LIRA addition (+4% over basal Ca^{2+} level, Additional file 4: Figure S4B). Thus, unlike pancreatic β-cells, acute GLP-1R stimulation in CD34$^+$ HSPCs did not significantly alter intracellular Ca^{2+}.

GLP-1R stimulation prevents CD34$^+$ HSPC dysfunction induced by chronic glucose overload

We recently published that metabolic stress induced by prolonged HG exposure results in loss of cell proliferation ability and CXCR4/SDF1-α axis impairment [14]. Herein, we tested whether LIRA, a GLP-1RA, was able to avert all these functional damages.

Despite the chronical exposure to HG concentration, LIRA dose-dependently (50 and 100 nM), prevented cell proliferation impairment. Noteworthy, the presence of 100 nM LIRA maintained cell proliferation rate to the control values (NG) (Fig. 4A and B). Similarly, LIRA treatment prevented CXCR4/SDF1-α axis defect promoted by HG exposure. Indeed, LIRA significantly maintained in dose dependent manner the migration ability of cells toward 50 ng/mL of SDF-1α (Fig. 4C) and CXCR4 expression (Fig. 4D and E).

LIRA reduces the oxidative state of CD34$^+$ HSPCs and metabolic imbalance promoted by HG exposure

We previously demonstrated that the loss of function promoted by HG-exposure was incident with mitochondrial ROS accumulation [14]. As shown in Fig. 5A and B, the maintenance of functional parameters despite HG presence was associated with a significant drug-induced reduction of cell oxidative state.

Moreover, HG-induced mitochondrial ROS accumulation was associated to oxidative metabolism dysfunction (Fig. 6). HG exposed CD34$^+$ HSPCs showed reduced maximal and spare MR, without significantly affecting basal MR. LIRA (100 nM) was able to restore maximal and spare MR to NG levels (Fig. 6A and Additional file 5: Figure S5A). Notably, neither HG-exposure nor LIRA treatment altered the percentage of the mitochondrial machinery used under basal conditions, as indicated by basal to maximal MR ratio, which remained constant

(See figure on next page.)

Fig. 2 GLP-1R expression in CD34$^+$ HSPCs. mRNA expression was assessed by RT-qPCR in 3 different CD34$^+$ HSPC biological replicates. An exon-exon spanning reverse primer was used to exclude any amplification of possible contaminating DNA; capan-1 cells were used as positive control (**A**). The identity of RT-qPCR products was determined by melting curve (**B**), agarose gel run (347 bp) (**C**) and finally by Sanger sequencing (**D**). CD34$^+$ HSPC lysates (40 µg) deriving from three biological replicates were immunoblotted in order to evaluate GLP-1R protein expression. Capan-1 cell lysate (20 µg) was used as positive control (**E**). S1, S2, S3 = samples 1, 2, 3

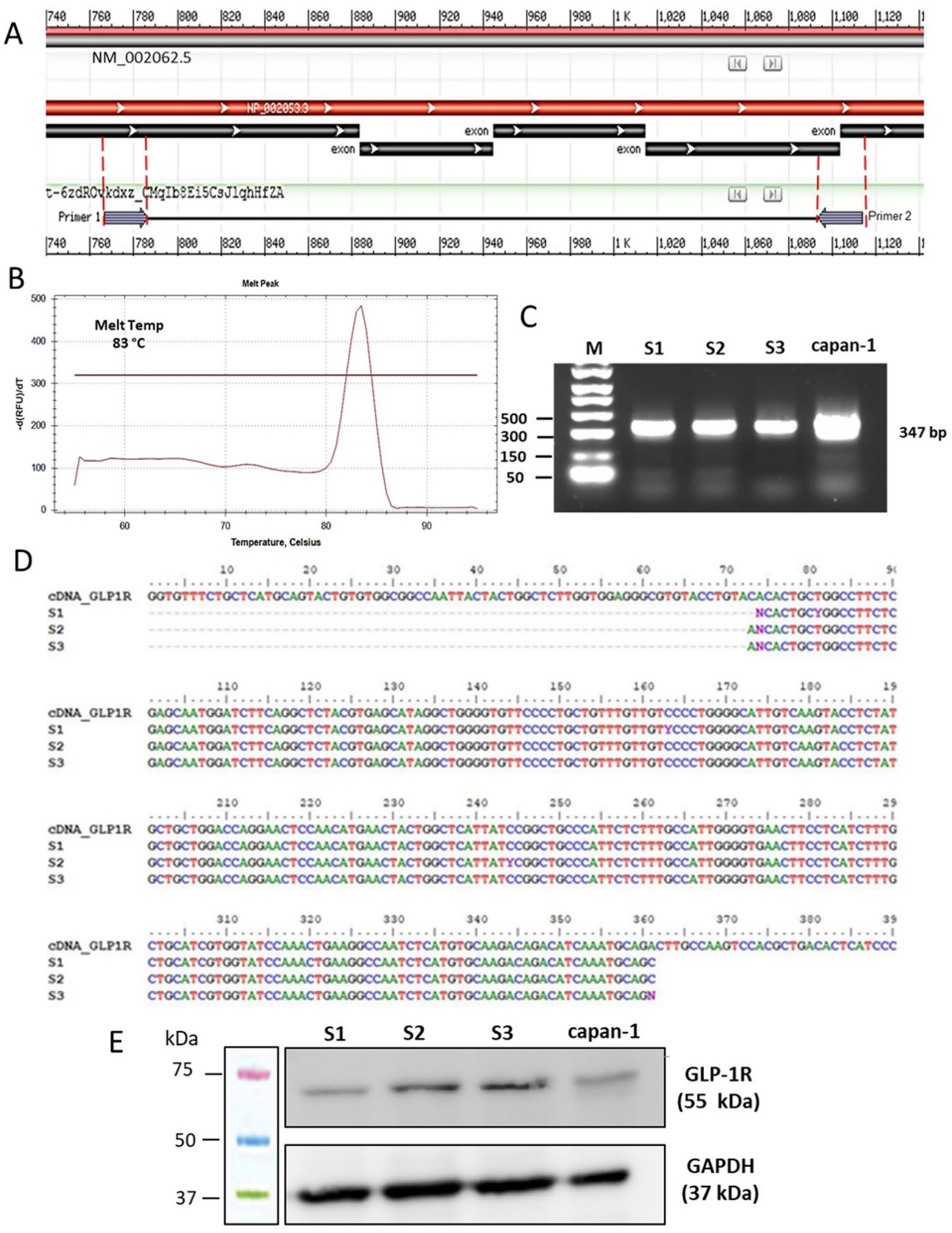

Fig. 2 (See legend on previous page.)

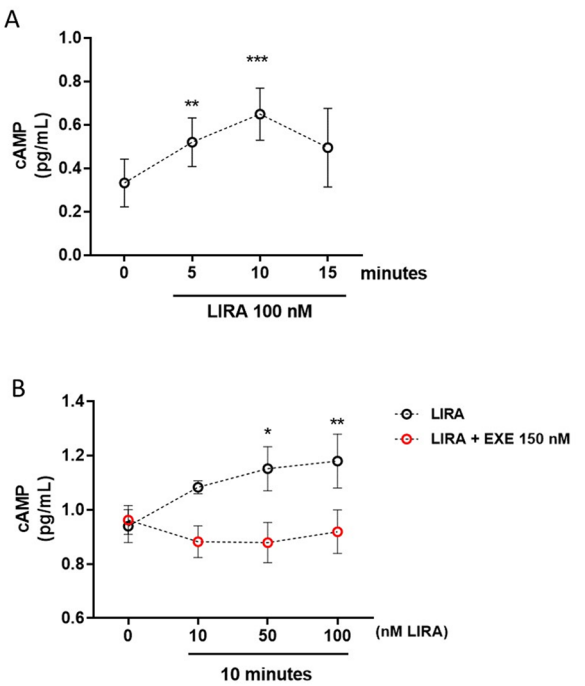

Fig. 3 GLP-1R downstream signaling pathway activation after stimulation by LIRA treatment. **A** CD34$^+$ HSPC stimulation with 100 nM LIRA determined a significant time-dependent accumulation of intracellular cAMP, with a maximum peak after 10 min of treatment (**p ≤ 0.01; ***p ≤ 0.001 *vs* basal; one-way ANOVA). **B** The addition of 150 nM EXE, a competitive antagonist of GLP-1R prevented the intracellular cAMP accumulation induced by increasing concentration of LIRA (10–100 nM) (*p ≤ 0.05, **p ≤ 0.01 *vs* basal two-way ANOVA). EXE = exendin 9–39, LIRA = liraglutide

in all groups. LIRA also restored the basal respiration devoted to ATP production (here reported as coupling efficiency, Fig. 6A). These effects of both HG and LIRA treatment were correlated to a trend in proton leak alteration (Additional file 5: Figure S5B). From the analysis of the glycolytic parameters, it emerged that HG-exposure increased the basal and maximal glycolysis and ATP produced via this metabolic route (Fig. 6B). Unlike the mitochondrial function, LIRA was unable to restore HG-induced glycolytic bioenergetic parameters changes to NG levels.

Overall, following HG exposure, LIRA treatment improved mitochondrial metabolism, stimulated ATP production via OXPHOS (Additional file 5: Figure S5C and S5D) and thereby increased the ATP rate index (Fig. 6).

GLP-1R stimulation promotes activation of ERK1/2 and PI3K signaling pathways

Stimulation of the GLP-1R is known to activate numerous pleiotropic signaling pathways in human pancreatic islet cells including PI3K and extracellular regulated kinases 1 and 2 (ERK1/2) [16, 17]. To determine whether the stimulation of endogenous GLP-1R expressed in CD34$^+$ HSPCs was also coupled to similar signal transduction pathways, we assessed the phosphorylation of ERK1/2 and AKT (a downstream effector of PI3K). As shown in Fig. 7A and C, stimulation of the cells with 100 nM LIRA elicited a time-dependent activation of both ERK1/2 and AKT kinases. LIRA-dependent kinase activation was abrogated by the addition of the two selective ERK1/2 and PI3K inhibitors: PD and WT, respectively (Fig. 7E and G).

These data indicate that CD34$^+$ HSPCs express a functional GLP-1R whose stimulation is coupled to additional signaling pathways other than adenylate cyclase.

Exendin (9–39) antagonizes LIRA effects against hyperglycemia

In order to confirm that LIRA-induced activation of diverse pro-survival signaling pathways was acting through GLP-1R activation, aforementioned experiments were carried out in the presence or absence of EXE antagonist (150 nM) [18]. As shown in Fig. 8A, EXE abrogated LIRA-dependent ERK1/2 and AKT phosphorylation as well as its protective effect on cell proliferation, measured as doubling time, (Fig. 8D) and CXCR4 membrane expression (Fig. 8E). Taken together, these findings support a GLP-1R-mediated effect of LIRA on intracellular pathways and functions of CD34$^+$ HSPCs.

LIRA partially recovers the functional damage induced by HG exposure in CD34$^+$ HSPCs

As we recently reported, a strong antioxidant machinery confers to CD34$^+$ HSPCs a particular resistance to HG-induced oxidative stress [14]. However, after antioxidant defense exhaustion, irreversible functional alterations take place. Here, in a different experimental setting (Fig. 1B), we aimed at investigating whether LIRA was also able to recover the compromised cell phenotype induced by HG exposure.

While 100 nM LIRA modestly improved HG-CD34$^+$ cell growth rate (Fig. 9A), we found that the same drug concentration significantly recovered CXCR4 membrane expression (Fig. 9B), and restored migration ability of the cells (Fig. 9C), although the latter less efficiently than when added concomitantly to HG. Again, these effects were associated with a significant drug-dependent reduction of intracellular ROS levels (Fig. 9D).

Discussion

CV complications remain the major cause of morbidity and mortality of patients with DM and first-generation glucose lowering agents have proved to be inadequate

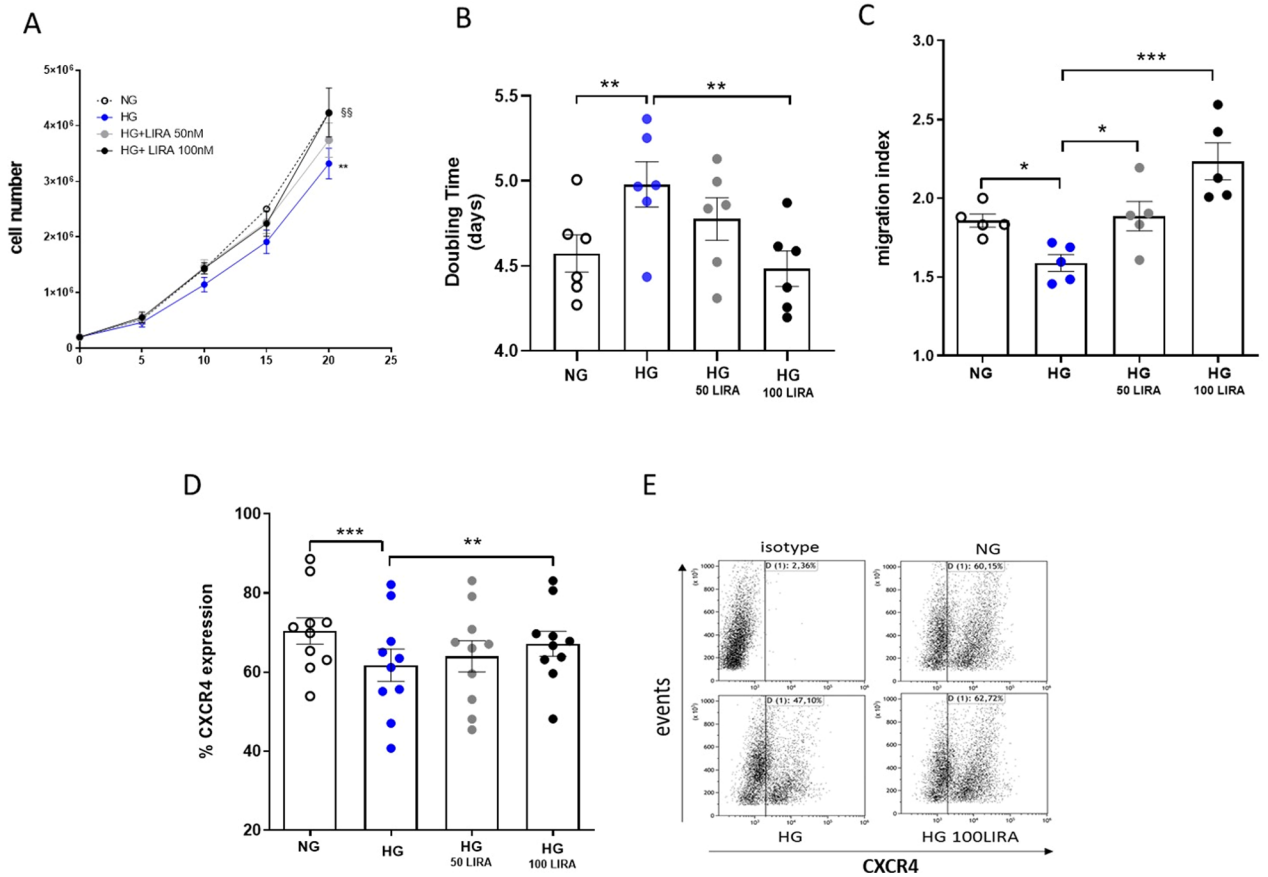

Fig. 4 LIRA treatment prevented CD34$^+$ HSPC proliferation, CXCR4/SDF-1α axis impairment and ROS accumulation caused by 20 days HG exposure. **A** Proliferation curve of CD34$^+$ HSPC amplified in NG, HG ± 50 nM and 100 nM LIRA conditions (**p ≤ 0.01 HG *vs* NG; §§ p ≤ 0.01 HG 100 LIRA *vs* HG; two-way ANOVA). **B** Doubling time of CD34$^+$ HSPCs cultured in NG, HG ± 50 nM and 100 nM LIRA (**p ≤ 0.01 HG *vs* NG; **p ≤ 0.01 HG 100 LIRA *vs* HG; one- way ANOVA). **C** CD34$^+$ HSPC migration towards SDF-1α (50 ng/mL) after NG, HG ± 50 nM and 100 nM LIRA treatment (*p ≤ 0.05 HG *vs* NG; *p ≤ 0.05 HG 50 LIRA *vs* HG; ***p ≤ 0.001 HG 100 LIRA *vs* HG; one-way ANOVA). **D** Analysis by flow cytometry of CXCR4 expression in NG, HG ± 50 nM and 100 nM LIRA treated CD34$^+$ HSPCs (***p ≤ 0.001 HG *vs* NG; ** p ≤ 0.01 HG 100 LIRA *vs* HG; one-way ANOVA). **E** Representative dot plot of CXCR4 cytofluorimetric analysis. HG = high glucose, LIRA = liraglutide, NG = normal glucose

[19] or only partially able to favorably impact CV prognosis [20]. Recently, large-scale trials unequivocally demonstrated the CV protective effects of two novel classes of glucose-lowering agents characterized by different dominant mechanism of action: sodium–glucose cotransporter-2 (SGLT2) inhibitors and GLP-1RAs. Both classes of drugs showed to significantly reduce the risk for MACE and all-cause mortality on top of standard of care in T2DM patients [8–10, 21, 22]. These CV benefits, independent from their glucose-lowering action, rely on the enrolment of different and not definitively understood mechanisms at multiple organ systems. Among the numerous pleiotropic actions of GLP-1RAs that favorably affect diabetes comorbidities, the metabolic changes of the patients are determinant. LIRA showed to improve beta cell function, especially in subjects treated with multiple daily insulin injection [23], and to ameliorate circulating metabolome, with particular regard to sphingolipids (e.g. ceramide) [24] and LDL metabolism, this latter by reduction of plasma PCSK9 level [25]. Collectively, these metabolic effects, along with a direct and complementary activity of the drugs at CV level, concur to the beneficial features of GLP-1RAs [26, 27]. Nevertheless, the existence of additional mechanisms has been postulated. CD34$^+$ HSPCs are known to play a central role in the maintenance of CV homeostasis by regulating vascular repair and regeneration [28–30]. The importance of CD34$^+$ HSPC biological functions on CV outcome [6] is supported by the common ontological origin of vascular and hematopoietic system [31]. Notably, Nandula and colleagues demonstrated that the amelioration of metabolic, CV and renal parameters of T2DM patients after canagliflozin therapy, a SGLT2 inhibitor, was associated with the improvement of CD34$^+$ HSPCs

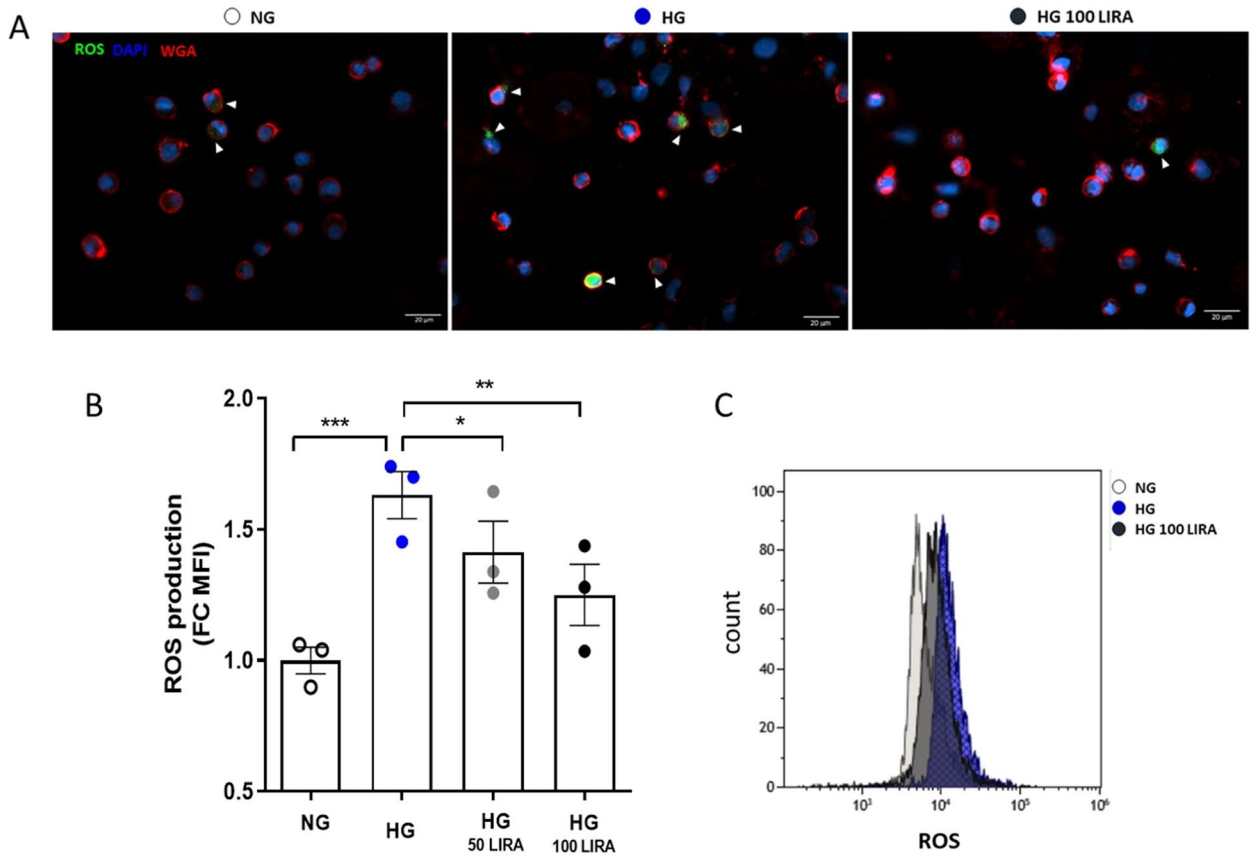

Fig. 5 Quantification of intracellular ROS level by immunocytochemistry (A) and flow cytometry (B) in NG, HG ± 50 nM and 100 nM LIRA treated cells (***p ≤ 0.001 HG *vs* NG; *p ≤ 0.05 HG 50 LIRA *vs* HG; ** p ≤ 0.01 HG 100 LIRA *vs* HG; one-way ANOVA). C) Representative flow cytometry histograms of intracellular ROS quantification. HG = high glucose, LIRA = liraglutide, NG = normal glucose

function [32]. Although different mechanisms of action are involved in CV protection of SGLT2 inhibitors, this study further supports the hypothesis that part of the mechanisms whereby GLP-1RAs improve CV outcome could rely on LIRA ability to reverse the functional impairment of $CD34^+$ HSPC provoked by HG.

$CD34^+$ HSPCs express a functional GLP-1R

We firstly provided unprecedented evidence that cord blood- and BM-derived $CD34^+$ HSPCs express GLP-1R (Fig. 2 and Additional file 3: Figure S3). The demonstration of GLP-1R expression by the identification of mRNA transcripts encoding for GLP-1R open reading frame and the use of validated antisera is often lacking and controversial in literature [33]. Therefore, to assess mRNA expression, we designed a couple of primers containing a reverse primer spanning an exon-exon junction. This granted the sole amplification of GLP-1R transcripts excluding any products deriving from possible DNA contamination, as we successfully confirmed by qPCR amplification of genomic DNA (data not shown). Afterwards, qPCR products were sequenced and aligned with the reference coding cDNA (NM_002062.5) confirming their identity. GLP-1R protein expression was finally detected by a top cited and validated antibody [34, 35], whose specificity was further proven in capan-1 cell lysate, a pancreatic cancer cell line expressing GLP-1R [36].

GLP-1R is a member of the secretin family or class B G protein-coupled receptors (GPCRs) [37]. Consistently with its canonical Gs mediated pathway activation, we showed that $CD34^+$ HSPCs express a functional GLP-1R. In fact, LIRA elicited a time- and dose-dependent accumulation of intracellular cAMP that was abrogated by the competitive receptor antagonist EXE (Fig. 3). Noteworthy, differently from what reported in pancreatic β-cells, we observed a weak intracellular intracellular Ca^{2+} mobilization, suggesting that, in $CD34^+$ HSPCs, Ca^{2+}-mediated signaling pathways may not be fundamental for the biological activity of the receptor [38] (Additional file 4: Figure S4).

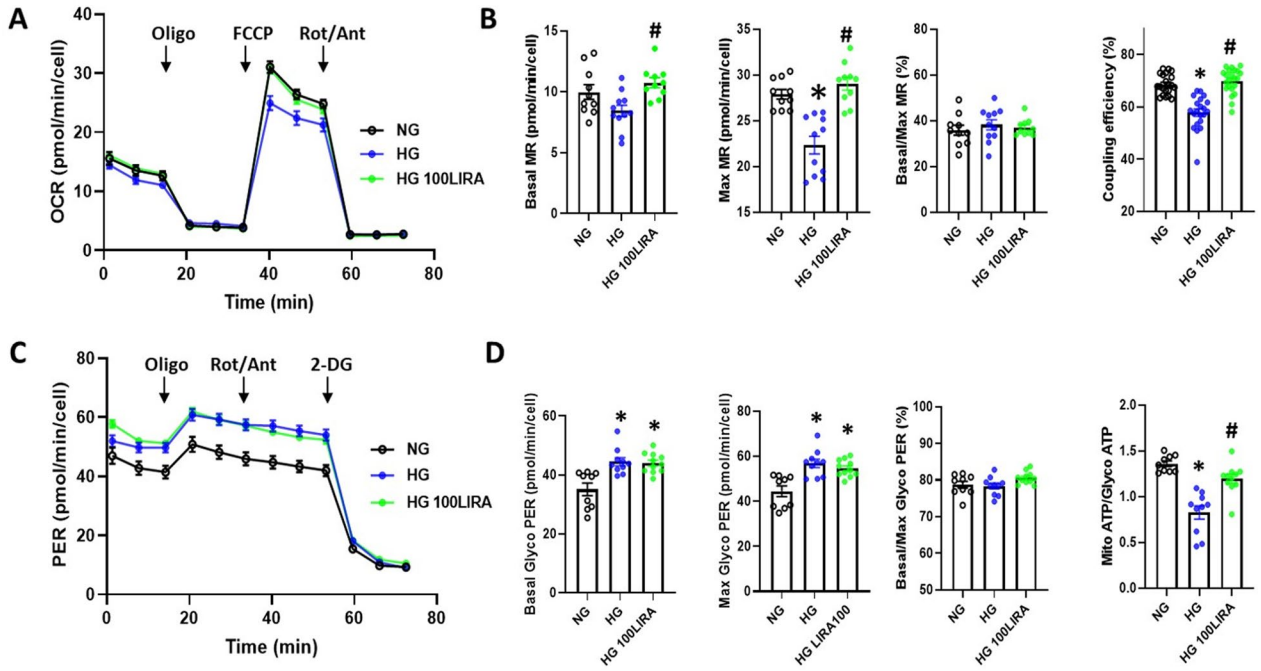

Fig. 6 LIRA recovered HG-damaged CD34$^+$ HSPC oxidative metabolism. Analysis of bioenergetics profiling with Seahorse in control (NG), after 20 days HG exposure alone (HG) or in the presence of 100 nM LIRA (HG 100LIRA). **A** Oxygen Consumption Rate (OCR) profiles of cells subjected to sequential injections of 1.5 μM oligomycin A, 2 μM FCCP and 0.5 μM rotenone + 0.5 μM antimycin A (XF Mito Stress Test protocol). OCR values were normalized to cell number by counting Hoechst-positive nuclei at the end of the experiment. **B** Statistics of mitochondrial parameters, including basal Mitochondrial Respiration (Basal MR), maximal Mitochondrial Respiration (Max MR), basal to maximal MR ratio and coupling efficiency. **C** Proton Efflux Rate (PER) profiles of cells subjected to sequential injections of 1.5 μM oligomycin A, 0.5 μM rotenone + 0.5 μM antimycin A and 50 mM 2-Deoxy-D-Glucose (combined XF ATP and Glyco rate protocols). **D** Statistics of glycolytic bioenergetic parameters, including basal Glycolysis (Basal GlycoPER), maximal Glycolysis (Max GlycoPER), basal to maximal GlycoPER ratio, ATP rate index (Mito ATP/Glyco ATP). *$p < 0.05$ vs NG, # $p < 0.05$ vs HG (one-way ANOVA plus Tukey's multiple comparison). Bioenergetic parameters were calculated from Seahorse data as described in Methods. Mean ± SEM from two individual experiments (n = 10–24 technical replicates). HG = high glucose, LIRA = liraglutide, NG = normal glucose

GLP-1R stimulation prevent HG-induced CD34$^+$ HSPC dysfunction and promotes mitochondrial metabolism

In the last years, a number of preclinical and clinical studies have demonstrated that native GLP-1 as well as GLP-1 RAs exert pleiotropic effects on different tissue subsets through both GLP-1R-dependent and independent mechanisms [27, 39]. At CV system level, they showed to improve endothelial function, reduce atherosclerosis, as well as oxidative stress and vascular and cardiac inflammation [27]. After GLP-1R expression in HSPC was confirmed, we were puzzled to evaluate its biological effects in a diabetic environment. We recently reported that the loss of glucose tolerance in CD34$^+$ HSPCs was associated with the reduction of proliferation rate, increase in mitochondrial ROS production and CXCR4/SDF-1α axis impairment [14]. These functional deficits are known to be primarily involved in the impairment of CD34$^+$ HSPC mobilization and migration capacity from the BM to sites of ischemia and endothelial injury in diabetic patients [40, 41]. Here we found that the concomitant administration of LIRA in HG setting was able to prevent HG-induced CD34$^+$ HSPC dysfunction and

(See figure on next page.)

Fig. 7 Intracellular pathway cross-talk after GLP-1R1 stimulation with 100 nM LIRA. **A** Representative immunoblots of ERK1/2 and **C** AKT phosphorylation in CD34$^+$ HSPCs treated with 100 nM LIRA for 5, 10 and 15 min and after the addition of MEK1/2 and PI3K selective pathway inhibitors, PD (**E**) and WT (**G**) respectively. GAPDH was used as loading control. **B**, **D**, **F**, **H** Immunoblotting quantification presented as arbitrary units after normalization to the GAPDH protein levels of three independent experiments. AKT = protein kinase B, ERK1/2 = extracellular signal-regulated kinases 1 and 2 GAPDH = Glyceraldehyde 3-phosphate dehydrogenase, LIRA = liraglutide, p-AKT = phospho-AKT, p-ERK1/2 = phospho-ERK1/2, PD = PD 98,059, WT = wortmannin

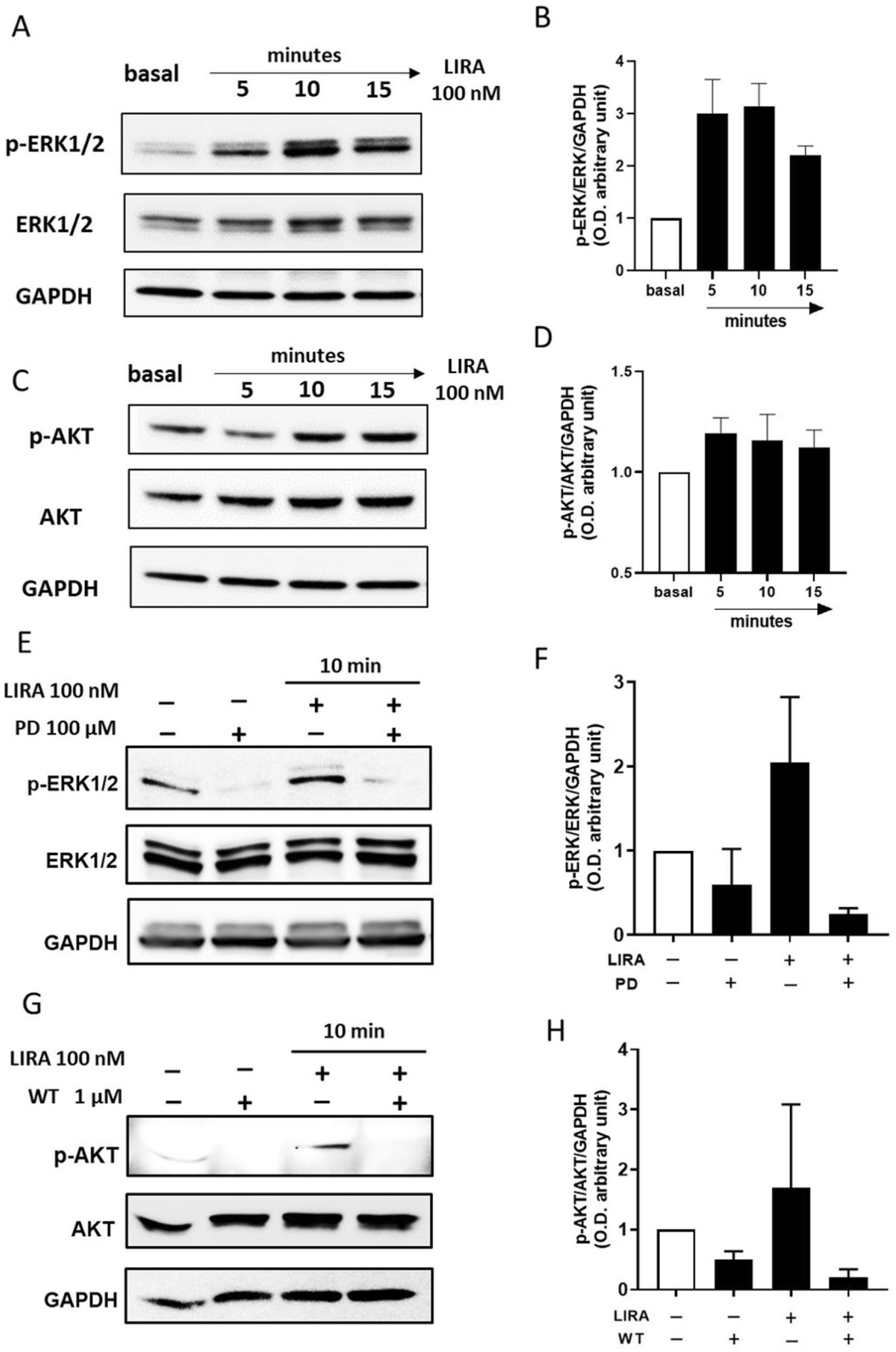

Fig. 7 (See legend on previous page.)

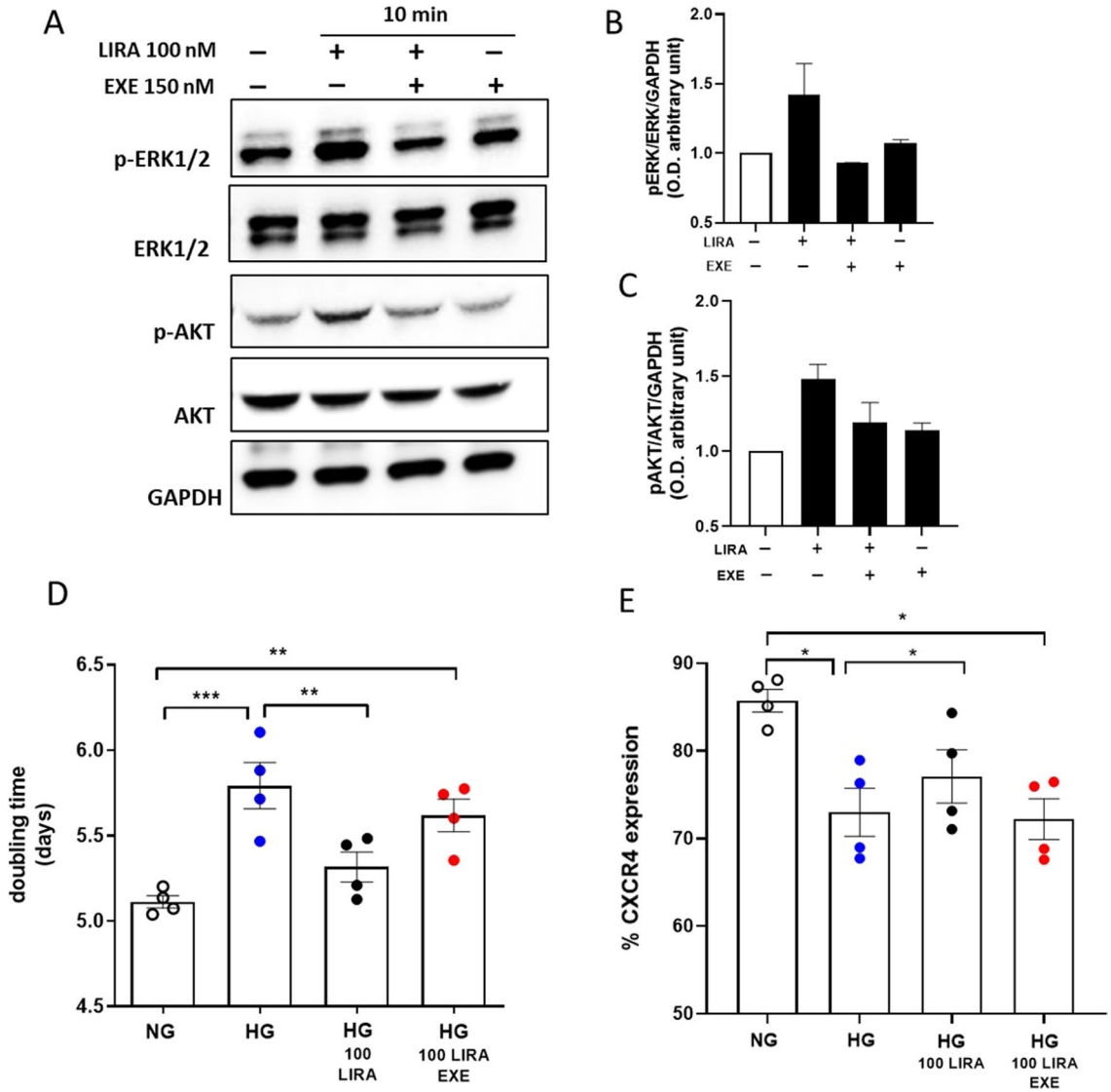

Fig. 8 The GLP-1R antagonist EXE abolished ERK1/2 and AKT phosphorylation as well as the protective effects promoted by LIRA treatment. **A** Representative immunoblot of ERK1/2 and AKT phosphorylation after stimulation with LIRA 100 nM ± EXE 150 nM for 10 min. GAPDH was used as loading control. **B**, **C** Immunoblotting results presented as arbitrary units after normalization to the GAPDH protein levels. **D** Doubling time of $CD34^+$ HSPCs cultured in NG, HG ± 50 nM and 100 nM ± EXE conditions (***$p \leq 0.001$ HG *vs* NG; ** $p \leq 0.01$ HG 100 LIRA *vs* HG; ** $p \leq 0.01$ HG 100 LIRA + EXE *vs* NG; one-way ANOVA. E) Analysis by flow cytometry of CXCR4 expression in NG, HG ± 50 nM and 100 nM ± EXE $CD34^+$ HSPCs (*$p \leq 0.05$ HG *vs* NG; *$p \leq 0.05$ HG 100 LIRA *vs* HG; *$p \leq 0.05$ HG 100 LIRA + EXE *vs* NG; one-way ANOVA). EXE = exendin 9–39, HG = high glucose, LIRA = liraglutide, NG = normal glucose

to improve their oxidative state (Figs. 4 and 5). It is well known that HG-induced overproduction of ROS can disrupt the mitochondrial membrane potential and damage mitochondrial function [42–45]. Seahorse analysis confirmed that exposure to HG of $CD34^+$ HSPCs induces a significant reduction of ATP produced by mitochondrial respiration (OXPHOS), as well as a reduced maximal and spare respiratory capacity. HG-exposed cells compensate for the impairment of mitochondrial function with an improvement of glycolytic ATP production, associated with increased basal and maximal glycolytic capacity. GLP-1R stimulation by LIRA affected cellular bioenergetics and restored mitochondrial function. These results further support the hypothesis that GLP-1RAs are able to reverse the functional impairment of $CD34^+$ HSPC provoked by HG.

Interestingly, in line with recent findings, the protective effects of LIRA persisted throughout the entire duration

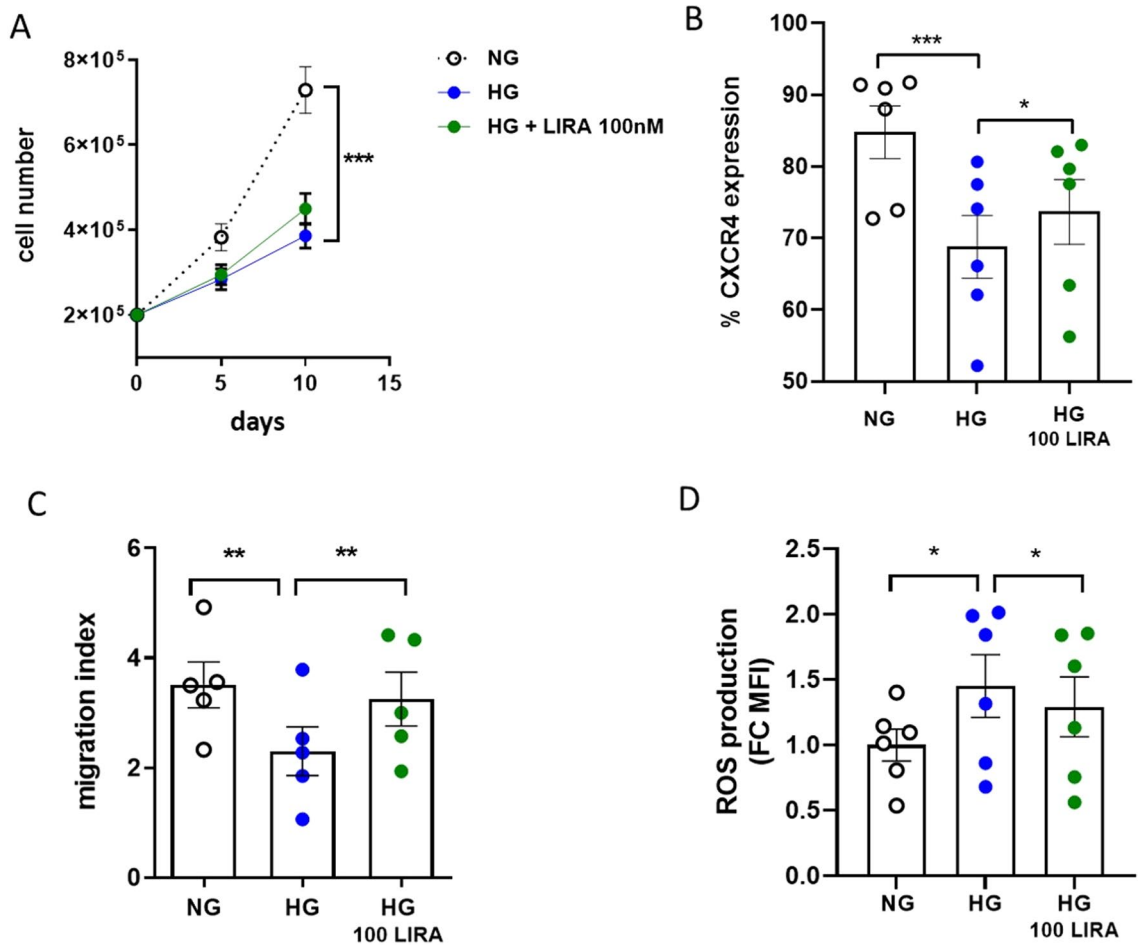

Fig. 9 LIRA partially recovered HG-damaged CD34$^+$ HSPC functions. **A** Proliferation curve of HG-damaged CD34$^+$ HSPCs after 10 days stimulation with 100 nM LIRA (***p ≤ 0.001 HG *vs* NG; two-way ANOVA). **B** Analysis by flow cytometry of CXCR4 expression level in HG-damaged CD34$^+$ HSPCs after 10 days of LIRA treatment (***p ≤ 0.001 HG *vs* NG; * p ≤ 0.05 HG 100 LIRA *vs* HG; one-way ANOVA). **C** Migration of HG-damaged CD34$^+$ HSPCs after 10 days of LIRA treatment (**p ≤ 0.01 HG *vs* NG; ** p ≤ 0.01 HG 100 LIRA *vs* HG; one-way ANOVA). **D** Quantification of intracellular ROS level by flow cytometry in HG-damaged CD34$^+$ HSPCs after 10 days of LIRA treatment (*p ≤ 0.05 HG *vs* NG; * p ≤ 0.05 HG 100 LIRA *vs* HG; one-way ANOVA). HG = high glucose, LIRA = liraglutide, NG = normal glucose

of the experiment, suggesting a sustained endosomal cyclic AMP generation induced by internalized activated receptor complex [46, 47].

GLP-1R stimulation promotes the activation of cytoprotective pathways

GLP-1R stimulation is known to promote transactivation of multiple intracellular pathways including PI3K, and ERK1/2. These pathways, which exert proliferative and cytoprotective functions [48], have been described in numerous extra glucose-lowering actions of incretins [39, 49]. In our hands, the treatment with 100 nM LIRA promoted in CD34$^+$ HSPCs a time dependent ERK1/2 and AKT phosphorylation that was completely abolished by the addition of PD 98059 and wortmannin, selective MEK1/2 and PI3K inhibitors respectively, and by the co-treatment with the GLP-1R antagonist EXE along with the related protective effects (Figs. 7 and 8). Albeit we are aware that we have not provided a full demonstration of the exact mechanism by which GLP-1R activation mediates ERK1/2 and AKT phosphorylation, we think we provided enough evidence that the protective effect of LIRA in CD34$^+$ HSPCs is mediated by GLP-1R, even if other mechanisms cannot be excluded.

According to guidelines, GLP1-RAs are now recommended to reduce the risk of CV events and mortality in T2DM patients. According to our hypothesis, this implies that LIRA cardiovascular protective effects are exerted after CD34$^+$ HSPC dysfunction has taken hold. To assess the ability of LIRA to recover a HG-related compromised

stem cell phenotype, the drug was given after the dysfunctional phenotype emerged. LIRA was able to recover $CD34^+$ HSPC function, even if less efficiently than early administration (Fig. 9). This observation corroborates accumulating evidence for supporting the use of GLP-1 RAs for CVD prevention in T2DM patients.

Conclusion

We provided first evidence that $CD34^+$ HSPCs express GLP-1R, and that the GLP-1RA LIRA prevents proliferation and migration impairment induced by chronic HG exposure. LIRA was also able to improve, even if less efficiently, $CD34^+$ HSPC function when previously exposed to HG conditions. Taken together these data suggest that the reported CV benefits of GLP-RAs can at least in part be related to cytoprotective effects on $CD34^+$ HSPCs.

Abbreviations

AKT/PKB: Protein kinase B; cAMP: Cyclic adenosine monophosphate; CB: Cord blood; CVD: Cardiovascular disease; ECAR: Extracellular acidification rate; ERK1/2: Extracellular signal-regulated kinases 1/2; EXE: Exendin fragment (9-39); FLT3: Fms-like tyrosine kinase 3; GLP-1: Glucagon-like peptide 1; GLP1-RAs: GLP-1 receptor agonists; HG: Hyperglycemic; IL: Interleukin; LIRA: Liraglutide; MACE: Major cardiovascular events; MEK1/2: Mitogen-activated protein kinase kinase; MR: Mitochondrial respiration; NG: Normoglycemic; OCR: Oxygen consumption rate; OXPHOS: Oxidative phosphorylation; PER: Proton efflux rate; PI3K: Phosphatidylinositol 3-kinase; PD: PD98059; PVDF: Polyvinylidene difluoride; ROS: Reactive oxygen species; SCF: Stem cell factor; SGLT2: Sodium–glucose cotransporter-2; T2DM: Type 2 diabetes mellitus; WT: Wortmannin.

Supplementary Information

The online version contains supplementary material available at https://doi.org/10.1186/s12933-022-01486-9.

Additional file 1: Figure S1 Flow-cytometric evaluation of sorted $CD34^+$ cell purity vs CD14 and CD3 cell contamination.

Additional file 2: Figure S2 A FCCP-uncoupled respiration (Maximal MR) and **B** coupling efficiency calculated from a Mito stress test assay performed on $CD34^+$ HSPC grown in NG, HG and HG 100 LIRA using different combinations of oligomycin A (0.5 and 1.5 μM) and FCCP (0.5, 1, 2 and 5 μM) to identify their minimal dose with the maximal response. Data were normalized to 0.5 μM oligomycin A + 0.5 μM FCCP to highlight differences. Mean ± SEM from one experiment (n = 4 technical replicates). Bars indicate statistical differences between groups (one-way ANOVA).

Additional file 3: Figure S3 GLP-1R expression in BM-derived $CD34^+$ HSPCs of T2DM patients. mRNA expression was assessed by RT-qPCR in 3 different biological replicates. The identity of RT-qPCR products was determined by agarose gel run (347 bp). M = marker; PZ1, PZ2, PZ3 = patient 1, 2, 3; B = blank.

Additional file 4: Figure S4 Intracellular Ca^{2+} mobilization in $CD34^+$ HSPCs w/wo GLP-1R stimulation. **A** Spontaneous Ca^{2+} transients elicited in single FLUO4 loaded cells before and during LIRA treatment. **B** Mean FLUO4 fluorescence before and after LIRA injection from a population of $CD34^+$ HSPCs (N = 8).

Additional file 5: Figure S5 Statistics of Spare Mitochondrial Respiration (**A**, Spare MR), Proton Leak (**B**), Mito ATP (**C**) and Glyco ATP (**D**) from ATP rate assay in all experimental groups. Mean ± SEM from two individual experiments (n = 10–24 technical replicates). *p < 0.05 vs NG, # p < 0.05 vs HG (one-way ANOVA plus Tukey's multiple comparison).

Acknowledgements

None.

Author contributions

AS and VV performed the experiments and were responsible for collection and compilation of data and in writing the manuscript. ER and GLP helped in performing Western Blot analysis, compilation of the data and in manuscript writing. EG helped in flow cytometry analysis. RR contributed in performing cellular experiments. MA, AB and MR performed intracellular calcium signaling analysis. AM and ES performed glucose metabolism analysis. PF, AR and GP revised the manuscript. SG designed and revised the manuscript. MCV designed, performed statistical analysis, supervised the study and revised the manuscript. All authors read and approved the final manuscript.

Funding

The study has been supported by Ricerca Corrente of Italian Ministry of Health (RC 2019 2764158 to Centro Cardiologico Monzino IRCCS) and 5 × 1000 Charity Fund.

Declarations

Ethics approval and consent to participate

Not applicable.

Consent for publications

Not applicable.

Competing interests

The authors declare that they have no competing interests.

Author details

[1]Unit of Vascular Biology and Regenerative Medicine, Centro Cardiologico Monzino IRCCS, Via C. Parea 4, 20138 Milan, Italy. [2]Department of Biotechnology and Biosciences, Università degli Studi di Milano-Bicocca, Milan, Italy. [3]Division of Endocrinology, ASST Fatebenefratelli-Sacco, Milan, Italy. [4]International Center for T1D, Pediatric Clinical Research Center Romeo ed Enrica Invernizzi, DIBIC, Università di Milano, Milan, Italy. [5]Nephrology Division, Boston Children's Hospital, Harvard Medical School, Boston, MA, USA. [6]Department of Biosciences, Università degli Studi di Milano, Milan, Italy. [7]Unit of Experimental Cardio-Oncology and Cardiovascular Aging, Centro Cardiologico Monzino IRCCS, Milan, Italy. [8]Department of Biomedical, Surgical and Dental Sciences, Università degli Studi di Milano, Milan, Italy. [9]Diabetes, Endocrine and Metabolic Diseases Unit, Centro Cardiologico Monzino IRCCS, Milan, Italy.

Received: 18 November 2021 Accepted: 2 March 2022
Published online: 09 April 2022

References

1. Saeedi P, Petersohn I, Salpea P, Malanda B, Karuranga S, Unwin N, Colagiuri S, Guariguata L, Motala AA, Ogurtsova K, et al. Global and regional diabetes prevalence estimates for 2019 and projections for 2030 and 2045: results from the International Diabetes Federation Diabetes Atlas, 9(th) edition. Diabetes Res Clin Pract. 2019;157:107843.
2. American Diabetes A. classification and diagnosis of diabetes: standards of medical care in diabetes-2018. Diabetes Care. 2018;41(Suppl 1):S13–27.
3. Pozzoli O, Vella P, Iaffaldano G, Parente V, Devanna P, Lacovich M, Lamia CL, Fascio U, Longoni D, Cotelli F, et al. Endothelial fate and angiogenic properties of human CD34+ progenitor cells in zebrafish. Arterioscler Thromb Vasc Biol. 2011;31(7):1589–97.
4. Fadini GP, Boscaro E, de Kreutzenberg S, Agostini C, Seeger F, Dimmeler S, Zeiher A, Tiengo A, Avogaro A. Time course and mechanisms of circulating progenitor cell reduction in the natural history of type 2 diabetes. Diabetes Care. 2010;33(5):1097–102.
5. Fadini GP. A reappraisal of the role of circulating (progenitor) cells in the pathobiology of diabetic complications. Diabetologia. 2014;57(1):4–15.

6. Fadini GP, Rigato M, Cappellari R, Bonora BM, Avogaro A. Long-term prediction of cardiovascular outcomes by circulating CD34+ and CD34+CD133+ stem cells in patients with type 2 diabetes. Diabetes Care. 2017;40(1):125–31.
7. Rigato M, Avogaro A, Fadini GP. Levels of circulating progenitor cells, cardiovascular outcomes and death: a meta-analysis of prospective observational studies. Circ Res. 2016;118(12):1930–9.
8. Marso SP, Daniels GH, Brown-Frandsen K, Kristensen P, Mann JF, Nauck MA, Nissen SE, Pocock S, Poulter NR, Ravn LS, et al. Liraglutide and cardiovascular outcomes in type 2 diabetes. N Engl J Med. 2016;375(4):311–22.
9. Marso SP, Bain SC, Consoli A, Eliaschewitz FG, Jodar E, Leiter LA, Lingvay I, Rosenstock J, Seufert J, Warren ML, et al. Semaglutide and cardiovascular outcomes in patients with type 2 diabetes. N Engl J Med. 2016;375(19):1834–44.
10. Gerstein HC, Colhoun HM, Dagenais GR, Diaz R, Lakshmanan M, Pais P, Probstfield J, Riesmeyer JS, Riddle MC, Ryden L, et al. Dulaglutide and cardiovascular outcomes in type 2 diabetes (REWIND): a double-blind, randomised placebo-controlled trial. Lancet. 2019;394(10193):121–30.
11. American Diabetes A. Cardiovascular disease and risk management: standards of medical care in diabetes-2021. Diabetes Care. 2021;44(Suppl 1):S125–50.
12. Cosentino F, Grant PJ, Aboyans V, Bailey CJ, Ceriello A, Delgado V, Federici M, Filippatos G, Grobbee DE, Hansen TB, et al. 2019 ESC guidelines on diabetes, pre-diabetes, and cardiovascular diseases developed in collaboration with the EASD. Eur Heart J. 2020;41(2):255–323.
13. Wei Y, Mojsov S. Tissue-specific expression of the human receptor for glucagon-like peptide-I: brain, heart and pancreatic forms have the same deduced amino acid sequences. FEBS Lett. 1995;358(3):219–24.
14. Vigorelli V, Resta J, Bianchessi V, Lauri A, Bassetti B, Agrifoglio M, Pesce M, Polvani G, Bonalumi G, Cavallotti L, et al. Abnormal DNA methylation induced by hyperglycemia reduces CXCR 4 gene expression in CD 34(+) stem cells. J Am Heart Assoc. 2019;8(9):e010012.
15. Drucker DJ, Philippe J, Mojsov S, Chick WL, Habener JF. Glucagon-like peptide I stimulates insulin gene expression and increases cyclic AMP levels in a rat islet cell line. Proc Natl Acad Sci USA. 1987;84(10):3434–8.
16. Trumper J, Ross D, Jahr H, Brendel MD, Goke R, Horsch D. The Rap-B-Raf signalling pathway is activated by glucose and glucagon-like peptide-1 in human islet cells. Diabetologia. 2005;48(8):1534–40.
17. Park S, Dong X, Fisher TL, Dunn S, Omer AK, Weir G, White MF. Exendin-4 uses Irs2 signaling to mediate pancreatic beta cell growth and function. J Biol Chem. 2006;281(2):1159–68.
18. Goke R, Fehmann HC, Linn T, Schmidt H, Krause M, Eng J, Goke B. Exendin-4 is a high potency agonist and truncated exendin-(9–39)-amide an antagonist at the glucagon-like peptide 1-(7–36)-amide receptor of insulin-secreting beta-cells. J Biol Chem. 1993;268(26):19650–5.
19. Zoungas S, Chalmers J, Neal B, Billot L, Li Q, Hirakawa Y, Arima H, Monaghan H, Joshi R, Colagiuri S, et al. Follow-up of blood-pressure lowering and glucose control in type 2 diabetes. N Engl J Med. 2014;371(15):1392–406.
20. Riddle MC. Modern sulfonylureas: dangerous or wrongly accused? Diabetes Care. 2017;40(5):629–31.
21. Rajagopalan S, Brook R. Canagliflozin and cardiovascular and renal events in type 2 diabetes. N Engl J Med. 2017;377(21):2098–9.
22. Zinman B, Wanner C, Lachin JM, Fitchett D, Bluhmki E, Hantel S, Mattheus M, Devins T, Johansen OE, Woerle HJ, et al. Empagliflozin, cardiovascular outcomes, and mortality in type 2 diabetes. N Engl J Med. 2015;373(22):2117–28.
23. Westman K, Imberg H, Wijkman MO, Hirsch IB, Tuomilehto J, Dahlqvist S, Lind M. Effect of liraglutide on markers of insulin production in persons with type 2 diabetes treated with multiple daily insulin injections. J Diabetes Complications. 2022;36(3):108110.
24. Jendle J, Hyotylainen T, Oresic M, Nystrom T. Pharmacometabolomic profiles in type 2 diabetic subjects treated with liraglutide or glimepiride. Cardiovasc Diabetol. 2021;20(1):237.
25. Verges B, Hassid J, Rouland A, Bouillet B, Simoneau I, Petit JM, Duvillard L. Liraglutide reduces plasma PCSK9 in patients with type 2 diabetes not treated with statins. Diabetes Metab. 2021;48(2):101284.
26. Sposito AC, Berwanger O, de Carvalho LSF, Saraiva JFK. GLP-1RAs in type 2 diabetes: mechanisms that underlie cardiovascular effects and overview of cardiovascular outcome data. Cardiovasc Diabetol. 2018;17(1):157.
27. Drucker DJ. The cardiovascular biology of glucagon-like peptide-1. Cell Metab. 2016;24(1):15–30.
28. Vinci MC, Bassetti B, Pompilio G. Endothelial progenitors: when confusion may give rise to new understanding. Int J Cardiol. 2020;318:121–2.
29. Sietsema WK, Kawamoto A, Takagi H, Losordo DW. Autologous CD34+ cell therapy for ischemic tissue repair. Circ J. 2019;83(7):1422–30.
30. Ballard VL, Edelberg JM. Stem cells and the regeneration of the aging cardiovascular system. Circ Res. 2007;100(8):1116–27.
31. Bertrand JY, Chi NC, Santoso B, Teng S, Stainier DY, Traver D. Haematopoietic stem cells derive directly from aortic endothelium during development. Nature. 2010;464(7285):108–11.
32. Nandula SR, Kundu N, Awal HB, Brichacek B, Fakhri M, Aimalla N, Elzarki A, Amdur RL, Sen S. Role of Canagliflozin on function of CD34+ve endothelial progenitor cells (EPC) in patients with type 2 diabetes. Cardiovasc Diabetol. 2021;20(1):44.
33. Drucker DJ. Incretin action in the pancreas: potential promise, possible perils, and pathological pitfalls. Diabetes. 2013;62(10):3316–23.
34. Katsurada K, Nandi SS, Sharma NM, Zheng H, Liu X, Patel KP. Does glucagon-like peptide-1 induce diuresis and natriuresis by modulating afferent renal nerve activity? Am J Physiol Renal Physiol. 2019;317(4):F1010–21.
35. Yu M, Agarwal D, Korutla L, May CL, Wang W, Griffith NN, Hering BJ, Kaestner KH, Velazquez OC, Markmann JF, et al. Islet transplantation in the subcutaneous space achieves long-term euglycaemia in preclinical models of type 1 diabetes. Nat Metab. 2020;2(10):1013–20.
36. Koehler JA, Drucker DJ. Activation of glucagon-like peptide-1 receptor signaling does not modify the growth or apoptosis of human pancreatic cancer cells. Diabetes. 2006;55(5):1369–79.
37. Mayo KE, Miller LJ, Bataille D, Dalle S, Goke B, Thorens B, Drucker DJ. International Union of Pharmacology. XXXV. The glucagon receptor family. Pharmacol Rev. 2003;55(1):167–94.
38. Yabe D, Seino Y. Two incretin hormones GLP-1 and GIP: comparison of their actions in insulin secretion and beta cell preservation. Prog Biophys Mol Biol. 2011;107(2):248–56.
39. Graaf C, Donnelly D, Wootten D, Lau J, Sexton PM, Miller LJ, Ahn JM, Liao J, Fletcher MM, Yang D, et al. Glucagon-like peptide-1 and its class B G protein-coupled receptors: a long march to therapeutic successes. Pharmacol Rev. 2016;68(4):954–1013.
40. Cencioni C, Capogrossi MC, Napolitano M. The SDF-1/CXCR4 axis in stem cell preconditioning. Cardiovasc Res. 2012;94(3):400–7.
41. Egan CG, Lavery R, Caporali F, Fondelli C, Laghi-Pasini F, Dotta F, Sorrentino V. Generalised reduction of putative endothelial progenitors and CXCR4-positive peripheral blood cells in type 2 diabetes. Diabetologia. 2008;51(7):1296–305.
42. Sivitz WI, Yorek MA. Mitochondrial dysfunction in diabetes: from molecular mechanisms to functional significance and therapeutic opportunities. Antioxid Redox Signal. 2010;12(4):537–77.
43. Sifuentes-Franco S, Pacheco-Moises FP, Rodriguez-Carrizalez AD, Miranda-Diaz AG. The role of oxidative stress, mitochondrial function, and autophagy in diabetic polyneuropathy. J Diabetes Res. 2017;2017:1673081.
44. Ni R, Zheng D, Xiong S, Hill DJ, Sun T, Gardiner RB, Fan GC, Lu Y, Abel ED, Greer PA, et al. Mitochondrial calpain-1 disrupts ATP synthase and induces superoxide generation in Type 1 diabetic hearts: a novel mechanism contributing to diabetic cardiomyopathy. Diabetes. 2016;65(1):255–68.
45. Kaludercic N, Di Lisa F. Mitochondrial ROS formation in the pathogenesis of diabetic cardiomyopathy. Front Cardiovasc Med. 2020;7:12.
46. Girada SB, Kuna RS, Bele S, Zhu Z, Chakravarthi NR, DiMarchi RD, Mitra P. Galphas regulates Glucagon-like peptide 1 receptor-mediated cyclic AMP generation at Rab5 endosomal compartment. Mol Metab. 2017;6(10):1173–85.
47. Jones B, Buenaventura T, Kanda N, Chabosseau P, Owen BM, Scott R, Goldin R, Angkathunyakul N, Correa IR Jr, Bosco D, et al. Targeting GLP-1 receptor trafficking to improve agonist efficacy. Nat Commun. 2018;9(1):1602.
48. Vinci MC, Visentin B, Cusinato F, Nardelli GB, Trevisi L, Luciani S. Effect of vascular endothelial growth factor and epidermal growth factor on iatrogenic apoptosis in human endothelial cells. Biochem Pharmacol. 2004;67(2):277–84.
49. Gupta V. Pleiotropic effects of incretins. Indian J Endocrinol Metab. 2012;16(Suppl 1):S47-56.

Publisher's Note